# High Performance Attitude Determination through Analysis of Geometric Distortions within Earth Observational Satellite Imagery

David Bamber, Dr Phil Palmer, Dr Stephen Mackin
Surrey Space Centre
University of Surrey, Guildford, Surrey, UK GU2 7XH; +44 1483 689278
D.bamber@eim.surrey.ac.uk, P.Palmer@eim.surrey.ac.uk, S.Mackin@eim.surrey.ac.uk

**ABSTRACT**
The application to which smaller and more affordable satellites may be employed is often constrained by the high pointing-accuracy requirements of current missions. There is therefore an increasing need to develop high accuracy attitude systems that do not breach small satellite mass and cost constraints. This paper proposes a novel method for determining attitude or rates over three axes using low cost, low mass, Earth-pointing push-broom sensor pairs. The technique is applicable to existing Low Earth Orbit (LEO) satellites with the appropriate camera systems, such as the Surrey Satellite Technology Ltd (SSTL) Disaster Monitoring Constellation (DMC) multispectral imager. The effects of attitude on satellite push-broom imagery are modelled, with inversions detailing the extraction of rates. Simulations show that using a suitable sub-pixel level registration scheme, such as Phase Correlation, with DMC imagery, attitude position accuracies in the order of a few arcminutes are achievable. Simulations have also shown pitch and roll rates of around an arcsecond per second to be measurable. Results using DMC imagery confirm the viability of using conventional, off-the-shelf, cameras onboard small satellites to determine attitude position and rates to a high level of accuracy.

## INTRODUCTION

The attitude determination and control system (ADCS), in addition to being critical to the success of a satellite mission, is one of the most expensive onboard systems, usually custom designed for specific spacecraft[1]. The mass and cost requirements of high accuracy ADCS often limit the pointing accuracy available for small satellite missions. For applications such as Earth observation, the quality of the imagery is constrained by such attitude stability requirements. This is recognised by ESA where: '*For some types of cameras (high-resolution 'pushbroom' scanners in particular), instantaneous attitude changes of even less than one arcsecond result in significant image distortion and blurring*'[2]. A need therefore exists for high accuracy attitude knowledge, especially during image capture, for small satellites.

The Surrey Space Centre, at the University of Surrey, has been investigating the effect of attitude perturbations on satellite imagery using Surrey Satellite Technology Ltd (SSTL) Disaster Monitoring Constellation (DMC). This paper explores the development of these studies and details a novel method for determining attitude position or rates over three axes in Low Earth Orbit (LEO) using Earth-pointing push-broom sensors. The high accuracies obtainable through this technique coupled with the sampling rates of push-broom technology also allow for analysis of onboard vibrations, *such as thermally induced high frequency jitter*. The technique requires two push-broom imagers, with CCD arrays, angled such that their ground projections form two near-parallel lines orthogonal to the direction of travel. The resulting time delay, for features at the front array to register at the trailing array, will allow for attitude-based image distortions, which can be discerned through registration of the resulting images.

Although much work has been done on image-based spacecraft pointing it is often related to rendezvous monitoring and flyby missions. JPL has recognized the need to identify, classify, and select planetary and celestial features for the realization of autonomous image-based spacecraft pointing systems and planetary flybys[3]. Casonata and Palmerini follow a similar line with trajectory monitoring systems for rendezvous between the Automatic Transfer Vehicle (ATV) and the international space station (ISS), where TV images have been used to determine the relative position and attitude[4]. In order to compensate for poor platform stability the European Space Agency (ESA) has proposed the use of an imaging system (SmartScan) to compensate for poor attitude stability. By allowing onboard analysis and correction of image-distortions, Smartscan hopes to establish the potential of such advanced sensor systems in future mission[2].

This paper models the effect of attitude positions and rates on satellite push-broom imagery and details the extraction of rates through inversion. Simulations show that using a suitable sub-pixel level registration scheme, such as Phase Correlation, with DMC imagery, attitude position accuracies in the order of a few arcminutes are achievable. Simulations have also

shown pitch and roll rates of around an arcsecond per second to be measurable. Image data collected during DMC attitude maneuvers prove the viability of the technique for measuring attitude, rates or onboard vibrations. The technique is applicable to existing Low Earth Orbit (LEO) satellites with the appropriate camera systems, such as a dual-bank single-band sensor pair from the DMC multispectral imager.

## DISASTER MONITORING CONSTELLATION

The Disaster Monitoring Constellation (DMC) comprises a network of five micro-satellites that have been built by SSTL with funding from an international consortium of nations[5]. The DMC spacecraft are equally spaced around a 686km 98° Sun-synchronous orbit. Through collaboration, the DMC is able to provide daily image coverage of any ground location with a 32m resolution and a 600km swath. The high temporal and spatial resolution coupled with the large swath of DMC is unique in allowing detailed coverage of events that would otherwise be missed.

### *Sensor Design*

The DMC satellites each have a multi-spectral imager (MSI) consisting of 2 banks of 3 channels pairs (Figure 1).

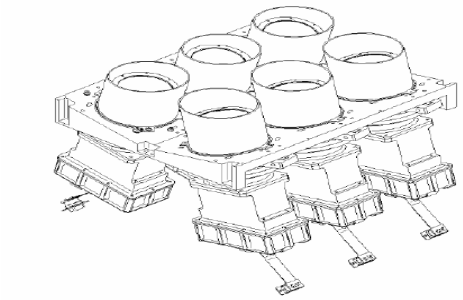

**Figure 1. Dual Bank DMC Channel Pairs**

The imager pairs each have linear CCD arrays, 10,000 pixels in length, with identical filters, providing three spectral bands in the ranges: 0.52-0.62 µm, 0.63-0.69 µm, and 0.76-0.9 µm. Each bank is mounted at an angle to the other to view adjacent parts of the ground, increasing the swath and giving a 19,500 pixel effective Field of View (FOV) to ensure daily revisit. The MSI is also designed to give an area of overlap of approximately 500 pixels between channel pairs, allowing continuity. In addition to the above, a small angular separation exists which, although within tolerances, allows features within the overlap to register at different times for different cameras.

### *ADCS*

Each DMC spacecraft is three-axis momentum bias stabilised and uses a Y momentum and Z reaction wheel, 3 orthogonal dual-wound magnetorquers and gravity gradient boom with 6-metre extendable tip mass for attitude control. The attitude determination sensors include 3-axis fluxgate magnetometer and 4 Sun sensors.

## METHODOLOGY

### *Registration Scheme*

Image registration is the process by which the most accurate match is found between two images of the same scene. Although a number of methods exist, most attempt to apply the optimum transform to one image ($f_A$) to better match the next ($f_B$). Such transforms are often measured through a series of inter-image shifts:

$$f_B(x,y) = f_A(x + x_0, y + y_0) \tag{1}$$

Where $x_0$ and $y_0$ represents the column and row shifts between two images, as measured in pixels, respectively. The accuracy of any image-based attitude estimates will be proportional to that of the registration scheme. Therefore, for the purposes of attaining high accuracy attitude estimates, this paper focuses on registration to a pixel and sub-pixel level, with two-dimensional shifts in mind. Shekarforoush's phase correlation method is a Fourier based approach to the registration problem with pixel and sub-pixel level accuracies attainable at relatively low computational cost, owing to the interpolation-free nature of the approach.

The phase correlation approach to image registration is based upon the shift theorem of Fourier transforms. According to Fourier shift theorem, when $F_B(\omega_x, \omega_y)$ is the Fourier transform of $f_B(x,y)$, then:

$$\frac{F_B(\omega_x,\omega_y)}{F_A(\omega_x,\omega_y)} = e^{j(\omega_x\Delta x+\omega_y\Delta y)} \tag{2}$$

Since we are only interested in phase shifts the cross power spectrum can be normalised, accounting for possible gain changes:

$$\frac{F_B(\omega_x,\omega_y)F_A^*(\omega_x,\omega_y)}{\left|F_B(\omega_x,\omega_y)F_A^*(\omega_x,\omega_y)\right|} = e^{j(\omega_x x_0+\omega_y y_0)} \tag{3}$$

where * denotes the complex conjugate.

For any two images with some degree of congruence, the inverse Fourier transform of the above cross power spectrum will contain a coherent peak that indicates the point of registration and incoherent peaks representative of noise power, normally distributed about a mean of zero.

Through analysis of the cross power spectrum under various sub-pixel shifts Shekarforoush[6] was able to suggest an interpolation-free approach to phase correlation registration. As the offset progresses from integer to sub-pixel level, the power in the correlation surface's coherent peak becomes shared with that of the neighbouring peaks. Through analysis of the ratio between neighbouring peaks Shekarforoush's approach was able to quantify the sub-pixel offset between imagery. The technique was tested with a host of aerial and satellite images and was found to estimate the shifts in registration to an accuracy of approximately 0.1 pixels (3σ).

***Image Registration based Attitude Model***

*Camera Frame*

For experimental purposes the sensor geometry is modelled on a single-band dual-bank camera pair from the DMC multi-spectral payload. Each of the three camera pairs is orientated to provide a 600km ground swath and 8km overlap. Figure 2 illustrates the relative orientation of the imaging planes for such a sensor pair in the area of overlap.

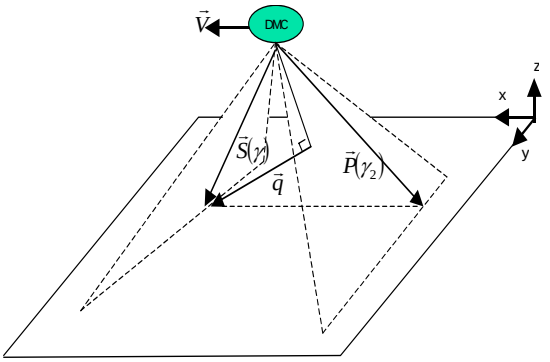


**Figure 2. Orientation of DMC Imaging Planes**

Let the camera's coordinate system be defined such that the X-axis is in the direction of flight, the Z-axis is away from the centre of the earth and the Y-axis completes the right-handed system. Within this frame the orientation of the port and starboard sensors can be nominally modelled with the following assumptions:

- The two CCD arrays are both within the plane defined by x =0
- The normal of each CCD array initially makes the angle β with the z-axis
- The optical axis of the starboard array is rotated about the sensor by the angle α and into the x-axis

This last assumption projects the starboard array ahead of the port creating a time delay between features registering at each array.

From this we can express the optical axis ( $\hat{X}v_C$ ) and CCD array ( $\hat{X}s_C$ ) of the trailing sensor (port) as:

$$\hat{X}v_C = \begin{bmatrix} 0 \\ \sin\beta \\ -\cos\beta \end{bmatrix} \quad \text{and} \quad \hat{X}s_C = \begin{bmatrix} 0 \\ \cos\ \beta \\ \sin\ \beta \end{bmatrix} \tag{4}$$

Using the cross product of $\hat{X}s_C$ and $\hat{X}v_C$ we can obtain a vector representative of the plane of the trailing array:

$$\hat{q}_C = \hat{X}v \times \hat{X}s = \begin{bmatrix} 1 \\ 0 \\ 0 \end{bmatrix} \tag{5}$$

As defined through the above assumptions the plane of the trailing array is a product of our y and z-axis. The unit vector $\hat{q}_C$ is normal to this plane and will therefore be defined by our x-axis within the camera frame. For the starboard array we can represent the projection of a single pixel as:

$$\hat{S}(\gamma_1)_C = \begin{bmatrix} \sin\alpha.\cos\gamma_1 \\ -\cos\alpha.\sin\beta.\cos\gamma_1 \\ -\cos\alpha.\cos\beta.\cos\gamma_1 + \sin\beta.\sin\gamma_1 \end{bmatrix} \tag{6}$$

Where $\gamma_1$ represents an angle across the plane of the starboard array's projection from its optical axis.

*Attitude Frame*

Let the orbital frame be defined such that under nominal attitude it is in alignment with the camera frame, with the x-axis along the velocity vector, the z-axis being away from the Earth and the y-axis completing the right handed system. With changes in attitude the camera frame becomes separated from the orbital frame by yaw ( $\mu$ ), pitch ( $\varpi$ ) and roll ( $\nu$ ), such that:

$$X_O = AX_C$$

With:

$$A = \begin{bmatrix} 1 & 0 & 0 \\ 0 & \cos\nu & -\sin\nu \\ 0 & \sin\nu & \cos\nu \end{bmatrix} \begin{bmatrix} \cos\varpi & 0 & -\sin\varpi \\ 0 & 1 & 0 \\ \sin\varpi & 0 & \cos\varpi \end{bmatrix} \begin{bmatrix} \cos\mu & -\sin\mu & 0 \\ \sin\mu & \cos\mu & 0 \\ 0 & 0 & 1 \end{bmatrix} \tag{7}$$

Where $X_O$ and $X_C$ represent projections in the orbital and camera frame respectively. With this, the projection of a pixel corresponding to $\gamma_1$ on the starboard array can be expressed as:

$$\hat{S}(\gamma_1)_O = A\hat{S}(\gamma_1)_C \tag{8}$$

If we assume the Earth surface to be a plane whose normal is parallel with our orbital z-axis then the projection of $\hat{S}(\gamma_1)_O$ onto the ground surface is:

$$\vec{S}(\gamma_1)_O = \frac{\hat{S}(\gamma_1)_O.h}{\hat{S}(\gamma_1)_O.\hat{k}} \tag{9}$$

Where *h* is representative of the altitude of the satellite above the plane of the Earth. With knowledge of $\vec{S}(\gamma_1)_O$, the distance between the ground projection of pixel $\gamma_1$ and the plane of the trailing array as measured along its normal can be calculated as:

$$|\vec{q}_O| = \vec{S}(\gamma_1)_O.\hat{q}_O \tag{10}$$

Where…

$$\hat{q}_O = \begin{bmatrix} \cos\varpi.\cos\mu \\ \cos\nu.\sin\mu - \sin\nu.\cos\mu\sin\varpi \\ \sin\nu.\sin\mu + \cos\nu.\cos\mu.\sin\varpi \end{bmatrix} \tag{11}$$

The time at which the plane of the trailing array crosses the pixel $\gamma$ can be calculated from the distance $|\vec{q}_O|$ and velocity at which the plane moves along $\hat{q}_O$:

$$\Delta T = \frac{|\vec{q}_O|}{|\vec{V}q_O|} \tag{12}$$

With:

$$\vec{V}q_O = \vec{V}_O.\hat{q}_O \tag{13}$$

With a push-broom camera the size and separation between successive rows of pixels is a function of time. The delay ΔT can therefore be used to determine the expected row shift ($\psi_R$) between front and trailing arrays for pixel $\gamma_1$:

$$\psi_R(\gamma_1) = \frac{\Delta T}{L_D} \tag{14}$$

Where $L_D$ is the Line duration as specified by the camera.

In order to ascertain the expected column shift between imagers given a yaw, pitch and roll, the point along the trailing sensor that crosses $\vec{S}(\gamma_1)_O$ must be found. This is achieved by projecting the starboard pixel $\gamma_1$ back along the ground plane with velocity $\vec{V}_O$ for the duration of the time delay *ΔT* such that:

$$\vec{P}(\gamma_2)_O = \vec{S}(\gamma_1)_O - \vec{V}_O.(\hat{i} + \hat{j})\Delta T \tag{15}$$

Where $\gamma_2$ represents an angle in the plane of the trailing array's projection across from its optical axis with:

$$\cos\gamma_2 = \frac{\vec{P}(\gamma_2)_O.\hat{X}v_O}{|\vec{P}(\gamma_2)_O|} \tag{16}$$

By then projecting the angles $\gamma_2$ and $\gamma_1$ up onto their sensors the position where feature $\vec{S}(\gamma_1)_O$ projects along each CCD array can be found. By comparing the displacement of features across from the optical axis along each array a measure for the column shift ($\psi_C$) of pixel $\gamma_1$ is predicted:

$$\psi_C(\gamma_1) = f(\tan\gamma_2 - \tan\gamma_1) \tag{17}$$

Where the focal length (*f*) in pixels is a function of the FOV and total number of elements along each CCD array (*N*):

$$f = \frac{N}{2.\tan\left(\frac{FOV}{2}\right)} \tag{18}$$

Using Equations 14 and 17 the expected row and column shift, given a yaw, pitch and roll, can be calculated. With the introduction of yaw, pitch and roll rates $(\mu r, \varpi r, \nu r)$ the orientation and velocity of the plane defined by $\hat{q}_O$ will vary with respect to time resulting in a deviation of $\vec{V}q_0$ and consequently $\Delta T$ from Equations 13 and 12, respectively. $\Delta T$ is then found by iteratively re-projecting the plane of the trailing array over a series of time steps converging at $|\vec{q}_O| = 0$ (The origin and orientation of the projected plane are time dependant). In practice a suitable threshold is reached within a few iterations as the error in row shift falls below the registration scheme accuracy. The column shift is then found through Equations 15 to 18 ensuring:

$$\hat{X}v_0 = \begin{bmatrix} 1 & 0 & 0 \\ 0 & \cos(\nu + \nu r.\Delta T) & -\sin(\nu + \nu r.\Delta T) \\ 0 & \sin(\nu + \nu r.\Delta T) & \cos(\nu + \nu r.\Delta T) \end{bmatrix}$$

$$\begin{bmatrix} \cos(\varpi + \varpi r.\Delta T) & 0 & -\sin(\varpi + \varpi r.\Delta T) \\ 0 & 1 & 0 \\ \sin(\varpi + \varpi r.\Delta T) & 0 & \cos(\varpi + \varpi r.\Delta T) \end{bmatrix} \tag{19}$$

$$\begin{bmatrix} \cos(\mu + \mu r.\Delta T) & -\sin(\mu + \mu r.\Delta T) & 0 \\ \sin(\mu + \mu r.\Delta T) & \cos(\mu + \mu r.\Delta T) & 0 \\ 0 & 0 & 1 \end{bmatrix}.\hat{X}v_C$$

## SIMULATIONS

Using the above model a series of simulations were implemented, in order to investigate how the row and column shifts along an array vary in accordance and relation to yaw, pitch, roll position and rates. Due to the angle $\beta$ the range of pixels across the array with obtainable shifts is confined to an area of overlap as defined by:

$$\delta = FOV - 2.\beta \tag{20}$$

Where $\delta$ represents the angular overlap, outside which pixels of alternate arrays do not correspond or register with one another.

The satellite altitude ($h$) and velocity ($V$) are assumed constant and equivalent to a DMC orbit[7], while the relative orientation of the camera pair is an exaggerated equivalent reaching 0.5 degrees $\alpha$. Unless otherwise stated, the $\beta$ angle is assumed equivalent to the angle between alternate DMC MSI banks.

### *Nominal Attitude and Rates*

With this, and under nominal attitude position and rates, the row and column shift will vary for each pixel across the array. This variation in row and column shift is representative of the varying distances and consequent delays between the ground projections of alternate imaging planes. This non-parallel relation is a function of $\beta$ and $\alpha$ with the angle between imager ground projections ($\theta$) under nominal attitude and rates being:

$$\theta = \sin^{-1}\left(\frac{\sin\alpha\sin\beta}{\sqrt{\sin^2\alpha\sin^2\beta+\cos^2\alpha}}\right) \tag{21}$$

The effect of the angle $\theta$ becomes more perceptible as the sensor's orientation increasingly deviates from nadir.

In order to better discern yaw, pitch and roll positions or rates this variation in row shift and column shift across the array must be appropriated in addition to the row and column shifts of individual pixels.

$$\rho_R = \frac{\psi_R(\gamma_B)}{\psi_R(\gamma_A)} \quad \text{and} \quad \rho_C = \frac{\psi_C(\gamma_B)}{\psi_C(\gamma_A)} \tag{22}$$

Where $(\gamma_B)$ and $(\gamma_A)$ represent pixel locations at opposite extents of the overlap.

### *Attitude*

A series of increasing yaw, pitch and roll positions were simulated individually, assuming nominal rates. At each position the row shift variation, column shift variation, column shift and row shift was appropriated and plotted (Figure 3 A & B).

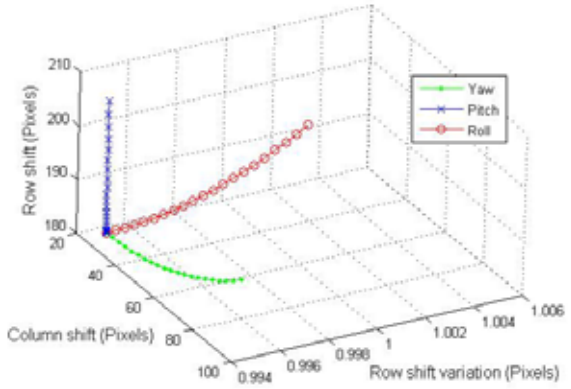


*(A)*

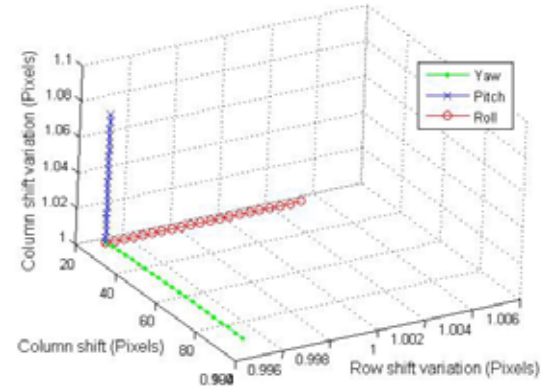


*(B)*

**Figure 3 (A & B). Effect of individual yaw, pitch or roll on inter-image geometry**

The row shifts and column shifts were determined using the pixel ($\gamma_P$) along the port array, which corresponds to nadir under nominal attitude. Whilst the intersections are representative of nominal satellite attitude each successive marker corresponds to an extra degree in yaw, pitch or roll, reaching 20 deg maximum.

The near orthogonal nature of Figure 3 shows that individual yaw, pitch and rolls are indeed separable using the above axes. Yaw and roll are primarily a function of column offset and row offset variation, respectively. Pitch position however can be discerned through analysis of either row offset or column offset variation, with the prior being more suitable due to the scales of sensitivity reflected in Figure 3. This relationship between platform orientation and geometric image distortions is reflected in Figure 4.

With deviations from nominal attitude the relative distances between different sections of each imagers ground projection becomes distorted, allowing pixels of the front array to register at differing sections of the trailing array and at different times. Following image registration such distortions take the form of the shifts seen in Figure 3.

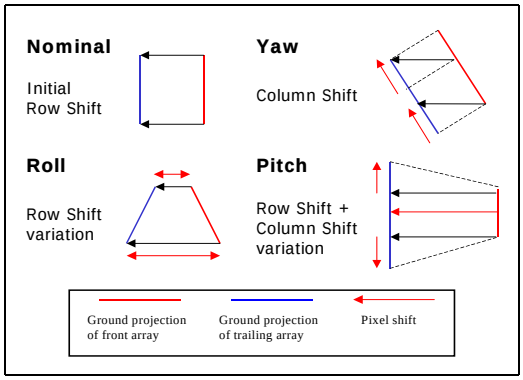


**Figure 4. Effect of attitude position on ground projection of alternate imaging arrays**

A series of consecutive yaw, pitch and rolls, reaching 40 degrees around each axis, were simulated and plotted using the above axis (Figure 5). Providing $\gamma_2 = \gamma_P$ the column shift will be invariant to any pitch or roll combination, and remain directly proportional to yaw position.

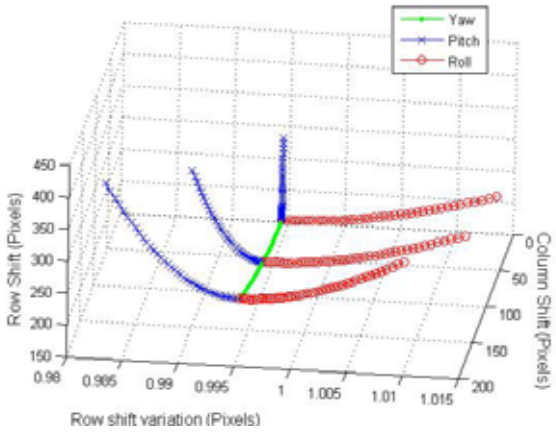


**Figure 5. Effect of consecutive yaw, pitch and roll on inter-image geometry**

Since rotators, such as in Equation 7, have a non-commutative nature the effect of a pitch or roll manoeuvre will be dependent upon the preceding yaw. This dependency is reflected in Figure 5 with a rotational exchange about the y-axis for any pitch or roll manoeuvre following increasing yaws. Pitch and roll can therefore be separated either through column shift variation, row shift variation or row shift, given the preceding yaw.

***Rates***

A series of yaw, pitch or roll rates were also simulated individually under nominal attitude position. The effect of each individual rate on the row shift, column shift, row shift variation and column shift variation is illustrated in Figure 6.

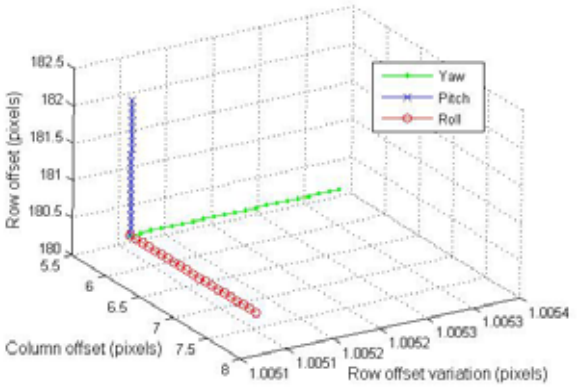


*(A)*

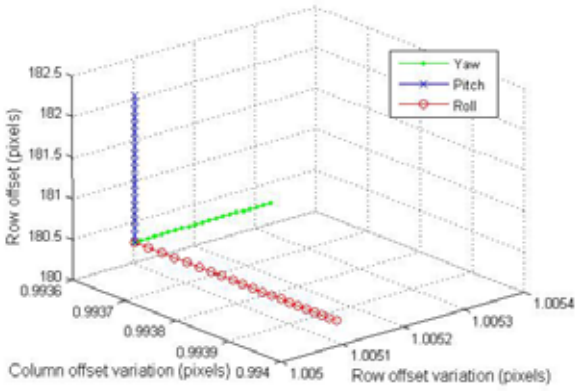


*(B)*

**Figure 6 (A &B). Effect of individual rates on inter-image geometry**

Each successive marker depicts an extra arcsecond per second in yaw, pitch or roll rate, reaching 20 arcseconds per second maximum. The near orthogonal alignment illustrated in Figure 6 (A & B) reflects the degree to which each rotational rate can be discerned using such axis. Through analysis of row shift and row shift variation the pitch rate and yaw rate can be discerned, respectively. The roll rate however, can be distinguished through observation of either column shift or column shift variation, with the prior being more preferable due to the scales of sensitivity. The effect of a given yaw rate on image geometry is small relative to the observable effects of roll rate or pitch rate.

***Summary***

Attitude position can be seen to create perspective-based distortions between the ground projections of alternate imagers. Attitude rates alter the direction and magnitude of the velocity vector along which the ground projection of alternate pixels may travel. Through analysis of the resulting shift in image geometry attitude position or rates may be determined. Table 1 details the axis of rotation that can be discerned using each image shift.

**Table 1. Discernable shifts in image geometry given attitude or rates**

| Image offsets | Rotation |
|---|---|
| Row offset | Pitch, Pitch rate |
| Column offset | Yaw, Roll rate |
| Row offset variation | Roll, Yaw rate |
| Column offset variation | Pitch, Roll rate |

## RATE INVERSION

Attitude rates are inherently simpler to extract from imagery than attitude position as the column and row shifts dictate where each pixel projection will be and at what time respectively.

The time taken ($\Delta T_P$) for a chosen port pixel projection ($\vec{P}(\gamma_{2P})$)to reach and register the corresponding point along the ground projection of the starboard array ($\vec{S}(\gamma_{1P})$) can be derived directly from the row shift of that pixel, with:

$$\Delta T_P = \Psi_R(\gamma_P).L_D \tag{23}$$

The point $\gamma_{1P}$ across the starboard array, where pixel $\gamma_{2P}$ will register at time $\Delta T_P$, can be seen as a function of the pixel's column shift, where:

$$\tan(\gamma_{1P}) = \frac{(f.\tan(\gamma_{2P}) - \Psi_C(\gamma_{2P}))}{f} \tag{24}$$

The velocity vector ($\vec{V}_P$) that defines the path of the projected pixel $\gamma_{2P}$ along the ground plane can therefore be found from:

$$\vec{V}_P = \frac{\vec{S}(\gamma_{1P}) - \vec{P}(\gamma_{2P})}{\Delta T_P} \tag{25}$$

If the velocity vectors $\vec{V}_A$ and $\vec{V}_B$, for pixels at opposite extremities of the overlap ($\delta$), are found and projected along for a duration $\Delta T_P$ then the orientation of the starboard imaging plane's ground projection can be mapped for that time. If the satellite position is also projected along its velocity vector for the equivalent duration then the plane of the starboard array can be defined through the projection of pixels $\vec{P}(\gamma_{2A})$ and $\vec{P}(\gamma_{2B})$ at time $\Delta T_P$ with:

$$\vec{P}(\gamma_{2A}^{\Delta Tp}) = \vec{P}(\gamma_{2A}) + \Delta T_P.(\vec{V}_A - \vec{V}_0) \tag{26}$$

and

$$\vec{P}(\gamma_{2B}^{\Delta Tp}) = \vec{P}(\gamma_{2B}) + \Delta T_P.(\vec{V}_B - \vec{V}_0) \tag{27}$$

From this, the direct cosine matrix ($A$), that separates $X_C$ from $X_O$ at time $\Delta T_p$, can be determined:

$$A = \begin{bmatrix} \hat{X}_i & \hat{X}_j & \hat{X}_k \\ \hat{Y}_i & \hat{Y}_j & \hat{Y}_k \\ \hat{Z}_i & \hat{Z}_j & \hat{Z}_k \end{bmatrix} \tag{28}$$

With:

$$\hat{Z} = -\hat{P}(\gamma_{2P}^{\Delta Tp})$$

$$\vec{X} = \hat{P}(\gamma_{2B}^{\Delta Tp}) \times \hat{P}(\gamma_{2A}^{\Delta Tp})$$

$$\hat{Y} = \hat{X} \times \hat{Z} \tag{29}$$

Where $\hat{X}$, $\hat{Y}$ and $\hat{Z}$ are orthogonal unit vectors that represent the orientation of the camera coordinate system relative to the orbit-defined coordinate system.

The yaw, pitch and roll at time $\Delta T_p$ can then be found through the parameterisation of the above, with:

$$\varpi^{\Delta Tp} = \sin^{-1}(\hat{X}_k)$$

$$\nu^{\Delta Tp} = \cos^{-1}\left(\frac{\hat{Z}_k}{\cos(\varpi^{\Delta Tp})}\right)$$

$$\mu^{\Delta Tp} = \cos^{-1}\left(\frac{\hat{X}_i}{\cos\varpi^{\Delta Tp}}\right) \tag{30}$$

The rate of rotational displacement along each axis can then be quantified from the observed changes in $\mu$, $\varpi$ and $\nu$ that occurs over the duration $\Delta T_p$. As $\vec{V}_A$ increasingly deviates from $\vec{V}_B$, in accordance with yaw rate, an increasing levels of extrapolation will be required as the row shift of such pixels are representative of differing time frames.

## ERROR ANALYSIS

The error of any image-based attitude estimate can be expressed as the level of rotational ambiguity resulting from discrepancies in shift equivalent to the expected level of mis-registration. From this, the potential errors in yaw and pitch position or pitch and roll rate can therefore be determined from the column and row shifts, respectively:

$$\sigma_{(\mu,\nu r)} = \frac{\sigma_R}{\psi_C(\gamma_P)'} \quad \text{or} \quad \sigma_{(\omega,\varpi r)} = \frac{\sigma_R}{\psi_R(\gamma_P)'} \tag{31}$$

Where $\sigma_R$ represents the accuracy of the registration in pixels and the denominators corresponds to the differential of the column or row shifts relative to the rotation of interest.

Roll position and yaw rate are determined using the ratio of row shifts between alternate edges of the imager overlap. If we assume the registration errors to be equal across the imager, then the errors in roll position or yaw rate resulting from such mis-registration can be calculated from:

$$\sigma_{(v,\mu r)} = \frac{\sigma_R}{\rho_R'} \cdot \frac{\sqrt{\left(\psi_R(\gamma_B)^2 + \psi_R(\gamma_A)^2\right)}}{\psi_R(\gamma_B)^2} \quad (32)$$

***Sampling Frequency***

While the rate at which telemetry can be obtained is dependant upon the line duration ($L_D$) of the camera system, each observation will be representative of attitude collected over a time frame equivalent to $\Delta T$. The sampling frequency ( $\omega_S$ ) in Hz can therefore be expressed as:

$$\omega_S = \frac{1}{\Delta T} \quad (33)$$

Increases in $h$ and $\alpha$ can respectively reduce the velocity of and exaggerate the along flight separation between ground projections of each imaging plane, allowing for significant enhancements in attitude position and attitude rate accuracies at the expense of equivalent losses in sampling frequency.

As the orientation of the imager-pair increasingly deviates from nominal attitude the sensitivity of the approach to attitude position will improve noticeably. This being especially true of roll and pitch as each is quantified through the analysis of perspective-based distortions between imager ground projections. A nominal separation between the camera and attitude frame will therefore enhance the accuracy of any attitude position estimates at the expense of a decrease in sampling rate.

Enhanced position and rate accuracy without consequent loss in sampling rate can be achieved however through improved along–track ($L_D$) and across track ($f$) resolution of the imaging system in conjunction with registration scheme accuracy. Increases in $\delta$ will also allow for increased accuracy in yaw rates and roll position without consequent losses in sampling frequency.

***Accuracies***

Yaw, pitch and roll rate accuracies were calculated using the above and with a 0.1 pixel level accuracy being assumed of the registration scheme (Table 2). Each rate assumes individual rotation from a nominal standpoint. In order to optimise the yaw rate accuracy the $\beta$ angle was assumed minimal such that the overlap ($\delta$) approaches the FOV of the DMC MSI.

**Table 2. Rate accuracies**

| **Manoeuvre** | Yaw rate | Pitch rate | Roll rate |
|---|---|---|---|
| **Accuracy** | 7 arcsec/sec | 1 arcsec/sec | 1 arcsec/sec |

The yaw, pitch and roll position accuracies were calculated for two separate cases (Table 3). In both cases simulated column shift, row shift and row shift variation were used to help discern the sensitivity of the image geometry to each individual rotation from nominal attitude.

**Table 3. Individual attitude accuracies using two separate camera pair configurations**

| **Manoeuvre** | **Yaw** | **Pitch** | **Roll** |
|---|---|---|---|
| Case A | 2 arcmin | 1 degrees | 2 degrees |
| Case B | 2 arcmin | 5 arcmin | 3 arcmin |

Case A adopts the previously defined assumptions of the camera system, with relative sensor pair orientation being representative of a single-band dual-bank sensor pair from the DMC's multi-spectral payload. Using these criteria, the highest accuracies are observed in yaw position. The relatively poor accuracy of roll and pitch are in part due to the initial platform orientation, and the large β angle between port and starboard imagers limiting the size of the overlap (δ).

In order to increase the accuracy of pitch and roll, Case B assumes a nominal 10° pitch and 10° roll separation between camera and attitude frames. While the α angle remains equal to Case A the β angle is assumed minimal such that δ approaches the FOV of DMC's multi-spectral payload, further enhancing the roll accuracy. Case B can be seen to reflect a dual-band single-bank sensor pair from the DMC's multi-spectral payload. From Table 3 it is evident that, unless the initial orientation and overlap angle is of a suitable size, then pitch and roll will remain difficult to discern relative to the accuracies attainable in yaw.

## CASE STUDY: DMC

***Approach***

In order to test the model a series of manoeuvres were applied along UK-DMC image runs. With each image run a single-band raw image was extracted from the port and starboard overlap of each imaging cameras. These images were segmented into a series of overlapping sections along the length of the DMC image run (Figure 7). Each section was then registered, port to starboard, using the phase correlation registration scheme to equate the changes in row and column shift for the length of the image. Since the port and starboard images are captured in rapid succession using similar cameras and perspective the inter-image congruency will be favour optimal accuracies.

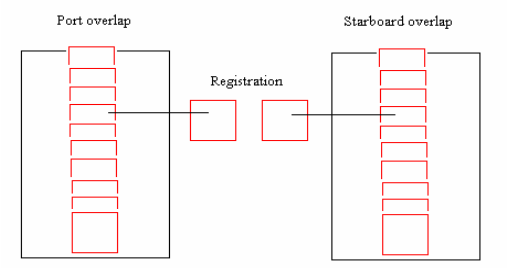


**Figure 7. Registration of DMC image segments**

The peak power of the cross power spectrum is also dependant upon the size of each image section registered in relation to scene texture. As the section size increases, aiding the inter-image congruence, high frequency data will become dampened, making optimal image section size difficult and, in some cases, scene dependant.

***Results***

In order to prove the potential of the system for measuring attitude position and rates, data from a yaw manoeuvre is analysed alongside data from an onboard vibration and pitch rate manoeuvre.

*Attitude Rates*

In order to test the ability of the model to detect and discern attitude rates, imagery captured during a Time Delay Integration (TDI) manoeuvre was analysed. This manoeuvre gave the satellite a pitch rotation of approximately 0.3 degrees per second, allowing the ground projection of alternate imaging planes to progress at approximately half normal pace. The imagery captured during this manoeuvre was registered and processed using the above registration technique and model inversions to extract the pitch rate. Figure 8 shows the pitch rate as extracted from a TDI and control image.

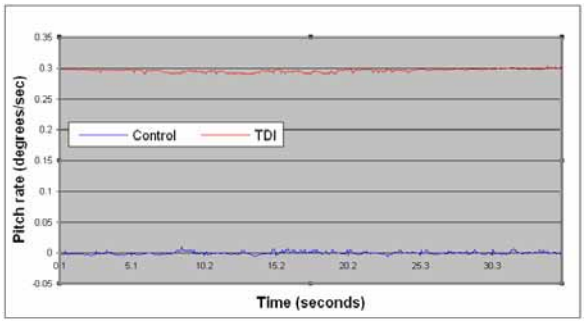


**Figure 8. Pitch Rate of Stationary and Rotating UK-DMC as Extracted from Imagery**

Both pitch rates were found to match onboard ADCS command rates, proving the potential of such a system for attitude rate estimation. The standard deviation of errors between simulated and actual shifts along the TDI image corresponded to approximately 10 arcseconds per second in pitch rate.

*Onboard Vibrations*

The technique has so far been tested on a host of DMC imagery. During analysis of a few select images, captured during the onset of the mission (2003), a periodic fluctuation in row and column shift was found along the imagery from alternate banks (Figure 9).

According to the image-based attitude model such oscillating shifts infer a periodic change primarily in pitch rate with a lesser flux in roll rate, indicative of a small onboard vibration along such axis.

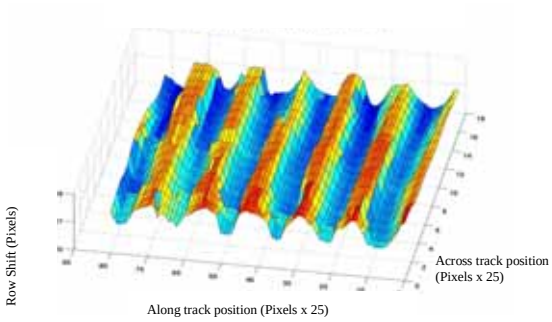


**Figure 9. Row Shift Oscillation across Image Scene**

Geo-rectification of the imagery has helped to corroborate the presence of this vibration with such onboard motion being observed as periodic changes in the velocity of each imaging plane. Figure 10 illustrates the variations in pitch rate, as extracted from such image scenes using the above model inversions.

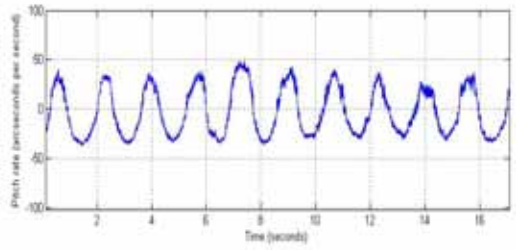

**Figure 10. Vibration Observed along DMC Image Run**

The vibration was found to have a frequency of approximately 0.6 Hz, which remained relatively consistent between scenes. Although the amplitude was found to vary it rarely exceeded 30 arcsecond per second in pitch rate or 15 arcsecond in absolute rotational displacement along the pitch axis, given the vibration frequency. The rate and scales of motion are respectively an order of magnitude too frequent and several orders too slight for onboard ADCS to register. Despite this, the motion is easily observed through analysis of along-scene inter-imager geometry. Although consecutive observations were sampled at an interval of 208 Hz, each measurement

relates to a time period an order of magnitude larger. According to the DMC's inter-imager geometry and given the phase-correlation registration accuracies, the accuracies of Figure 10 can be seen as approximately 5 arcseconds per second.

In an attempt to initiate the vibration observed in previous imagery the platform's y-axis momentum wheel was switched off and then reactivated part way along a DMC imaging run. The imagery from alternate banks was then registered using the above-mentioned techniques and inversions in order to extract the rate data. As seen in Figure 11, a vibration, operating primarily along the pitch axis, was observed subsequent to wheel activation.

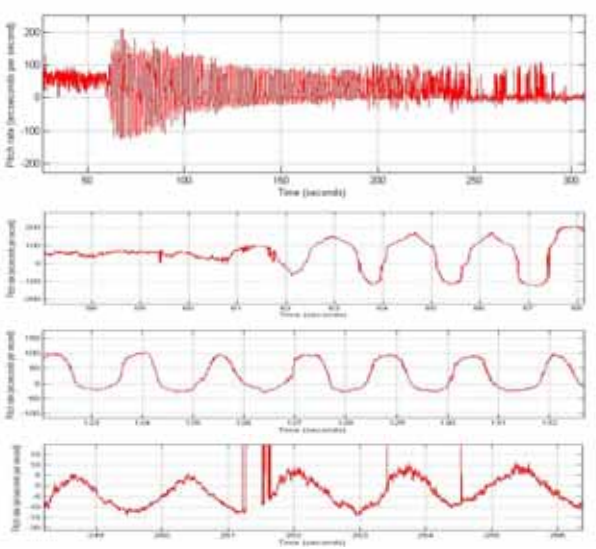

**Figure 11. Effect of y-axis Momentum Wheel Activation**

The frequency was found to coincide with that of vibrations from previous imagery. The amplitude of the vibration initially registered higher than previously recorded and then dissipates to levels beyond the sensitivity of this technique to detect over a period of approximately 300 second. The evolution and gradual decay of the vibration is clearly evident in Figure 11, with low-level fluctuations in pitch rates remaining discernable after 250 seconds.

*Attitude Position*

The z-axis momentum wheel was also deactivated prior to the above imaging run, but kept inactive for the duration of the scene. As a result, the satellite attitude was found to drift along such axis, reaching approximately 8 degrees yaw towards the extent of the imagery. The degradation in yaw was clearly apparent in the image geometry as a gradual increase in column shift for each pixel across the array. Simulations have shown that for pixel $\gamma_P$, which corresponds to nadir under nominal attitude, the column shift is invariant to pitch position and roll position. Assuming nominal rates, the yaw position can therefore be directly associated with column shift. From this, and with inter-imager geometry being known, yaw estimates were extracted along the observed image scene using a series of simulations and look-up-tables.

Figure 12 illustrates such image-geometry based yaw estimates as plotted alongside onboard ADCS data. While onboard ADCS telemetry is sampled at 0.2Hz, the frequency of acquisition for the below image based attitude observations corresponds to approximately 15Hz.

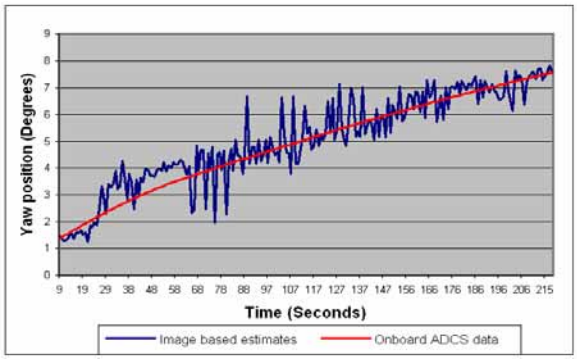


**Figure 12. Actual Drift in Yaw Vs Image-based Estimates**

A series of oscillations were observed alongside the general increase in yaw position. The frequency of these periodic fluctuations was found to match that of the above-mentioned momentum wheel based vibration. Such perturbations are likely a result of fluctuating roll rates, induced as the above-mentioned vibration operates, to some extent, across the satellite x-axis.

Image-based attitude position estimates were generally found to match the increasing trend of onboard observations endorsing the viability of the approach to discern discrepancies in yaw position. As seen in Figure 13 a high degree of congruency, reaching 0.96 in correlation coefficient, was observed between estimated and real data points.

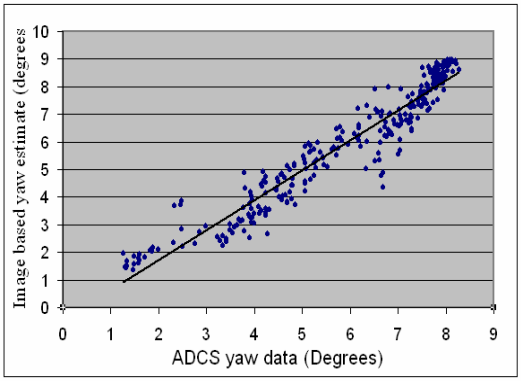


**Figure 13. Correlation between Estimated and ADCS Yaw Data**

Although, the standard deviation of yaw errors corresponded to approximately 0.6 degrees yaw, higher accuracies are envisaged through better separation of rates from attitude position.

## DISCUSSION & CONCLUSION

A method for obtaining high accuracy attitude data using low cost, low mass push-broom sensors in LEO has been proposed. A model has been created to help simulate the effect of attitude manoeuvres on imagery from such sensors. A method detailing the extraction of attitude rates has been suggested, which although simplistic in nature allows for precise rate data, given sufficient overlap between imagers. Simulations have shown that, with an orbit and camera system equivalent to that of the DMC micro satellite, and through analysis of across-track variations in row and column shift, attitude positions or rates can be distinguished over 3-axis. Initial results from registration of DMC imagery agree with the model and prove the viability for measuring absolute attitude position in addition to rates. Results have shown the approach to be approximately two orders of magnitude more sensitive to rates than position however.

The technique has shown potential to surpass most positional attitude system accuracies with the exception of the star camera. Contrary to Earth horizon or Sun sensors, the highest position accuracies are found in yaw, with 2 arc-minute measurements being achievable given the above criteria and suitable registration scheme. Roll and pitch accuracies can attain a few arc-minutes position given nominal separation of the camera frame from the body frame and an adequate $\delta$ angle.

The discernable level of change in roll and pitch, equated over a time frame equivalent to $\Delta T$, is respectively equivalent to the proportion of across-track and along-track IFOV that can be perceived using the appropriate registration scheme. With a DMC MSI and robust phase correlation registration this corresponds to an arc-second of angular displacement.

Onboard vibrations beyond the capability of many micro-satellite ADCS to discern have been detected and found to be clearly visible across the image run. The high attitude rate accuracies coupled with high sampling rates suggests the potential for gyroscope substitution or calibration.

Despite the above, it must be remembered that the results seen throughout this report are conservative with minimal filtering. Extensions to the phase correlation scheme have achieved accuracies in excess of 0.01 pixels[8]. This coupled with a camera system of a few metres ground resolution would allow the previously stated attitude position and rate accuracies to be enhanced by a factor of 100, without any degradation in sampling frequency. Such enhancement would allow for absolute attitude and rate accuracies in the order of an arcsecond and 0.01 of an arcsecond per second, respectively. While observations can be obtained at a frequency of over 200 Hz, registration displacement errors form a normal distribution about zero. There therefore exists further scope for enhancement of accuracies through filtering and integration of neighbouring data points.

In addition to the above benefits of a push broom sensor based attitude determination system there exists a number of limitation, a synopsis of which is detailed in Table 4. The above simulations, model inversions and attitude extractions currently remain untested with onboard systems. It is therefore important to recognise that although the required level of processing remains relatively computationally un-intensive, as onboard processing and power requirements are beyond the scope of this paper such constraints are unrealised.

If we are to consider the extraction of attitude rates and position from the geometric distortions between imager pairs then the number of unknowns begins to surpass the available degrees of freedom. The positions and rates can be decoupled however if additional sensor pairs are mounted such that their nominal orientations within the camera frame differ by sufficient relative rotational displacement.

**Table 4. Benefits of Pushbroom-based Attitude Determination**

| Advantages | Disadvantages |
|---|---|
| Discerns attitude position and rates over 3 axis | Attitude position and rates need decoupling |
| High accuracies and frequent acquisition rates | Dependency on image texture limits accuracy and orbital coverage |
| Off-shelf components allow for low costs and mass | Onboard power consumption and processing requirements unknown |

The accuracy of the registration scheme and consequent attitude estimates is highly dependant upon the scene texture. Although the registration technique has been found to functions adequately over a variety of ground terrains, the registration accuracy degrades over ocean, ice, clouds and non-sunlit portions of the orbital period. Although this is partly owing to the fact that DMC sensors are not normally trained to discern such features there exists the potential for improved registration through reselection of sensor saturation and gain levels or alteration of spectral resolution given a more optimal sensor system. Also, if the attitude technique were to be implemented whilst in orbit of a body other than that of the Earth, such as the Moon or Mars, then the lack of large water bodies and dense atmosphere would only aid in accuracy of system.

In summary, this report has proven the viability of using conventional, off-the-shelf, cameras onboard small satellites to determine attitude position and rates to a high level of accuracy. The accuracies achievable compete with and surpass most current ADCS accuracies and rates of acquisition suggesting the potential of the approach to form the backbone of future alternate ADCS systems. Since the technique is capable of working with conventional onboard cameras, the cost and additional mass of such a system is deemed negligible. For small satellite missions that require high pointing accuracies, cost and mass constraints are paramount. With further study, the potential of this technique for substitution of existing attitude systems, with great savings in mass and cost, may be realised.

**ACKNOWLEDGEMENTS**

This research was funded by Surrey Space Centre which is a part of the University of Surrey. Thanks to Gary Crowley, Dave Hodgson, James Wilhelm and Neville Bean for their scheduling and data supply assistance and to DMC International Imaging Ltd for all their help and advice relating to DMC imagery.

**REFERENCES**

1. F. Marteau, S. B. Gabriel, E. Rogers, "Attitude Determination and Control for Small Satellites", in UKACC International Conference on Control 1996, IEE, pp. 620-625, 2-5 September 1996.

2. V. Tchernykh, S. Dyblenko, K. Janschek; K. Seifart; B. Harnisch, "Clever Imaging with SmartScan", in ESA bulletin 123, pp. 40-45, August 2005.

3. C. Chu, D. Q. Zhu, S. Udomkesmalee, M. I. Pomerantz, "Realization of autonomous image-based spacecraft pointing systems : planetary flyby example", in SPIE's International Symposium on optical Engineering in Aerospace Sensing, Space Guidance, Control and Tracking Conference, Paper No. 2221-04, Orlando, FL, 4-8 April, 1994.

4. G. Casonato, G. B. Palmerini, "Visual Techniques Applied to the ATV/ISS Rendez-Vous Monitoring", IEEE Aerospace Conference Proceedings, pp. 613-625, 2004.

5. Stephens, P.; Cooksley, J.; da Silva Curiel, A.; Boland, L.; Jason, S.; Northham, J.; Brewer, A.; Anzalchi, J.; Newell, H.; Underwood, C.; Mackin, S.; Sun, W.; Sweeting, S.M., **"**Launch of the international Disaster Monitoring Constellation**",** Recent Advances in Space Technologies, 2003. RAST '03, 525 – 535, 20-22 Nov, 2003.

6. H. Shekarforoush, M. Berthod, and J. Zerubia, "Subpixel image registration by estimating the polyphase decomposition of cross power spectrum", in Proceedings 1996 IEEE Computer Society Conference on Computer Vision and Pattern Recognition, USA, June 1996, pp. 532-537, IEEE.

7. Ward, J.; Jason, S. and M. Sweeting, "Microsatellite Constellation for Disaster Monitoring," Proceedings of the 13th Annual Small Satellite Conference, Utah, 1999.

8. Averbuch, A. and Y. Keller, "FFT based image registration", in Proceedings 2002 IEEE Conference on Computer Vision and Pattern Recognition, September 2002, IV, pp.3608-3611, IEEE.